Universidade de São Paulo
Instituto de Astronomia, Geofísica e Ciências Atmosféricas
Departamento de Astronomia

Lucas Gabriel Silva

Photometric estimator of galaxy cluster masses

São Paulo
2023

Lucas Gabriel Silva

Photometric estimator of galaxy cluster masses

Trabalho de Conclusão de Curso apresentado ao Instituto de Astronomia, Geofísica e Ciências Atmosféricas da Universidade de São Paulo como requisito parcial para a obtenção do título de Bacharel em Astronomia.

Vertente: Pesquisa Básica
Orientador: Prof. Dr. Laerte Sodré Jr

São Paulo

2023

To Maria, beloved grandmother. I wish we had more time together.

Acknowledgements

There are many people who deserve to be thanked for this achievement. However, I would like to express my deepest gratitude and love to my mother, Cristiane. She is an incredibly strong and kind person who fights every day to ensure that I experience the best that life has to offer. She is always the first person I want to share my accomplishments with, and the greatest joy for me is seeing her proud smile when I do it. Mom, I have big dreams in life, but the biggest one is to one day tell you that every battle was worth it. Nevertheless, along this journey, I hope to see that smile several times.

I would also like to express my heartfelt appreciation to my advisor, Laerte Sodré. None of this would have been possible without his guidance and support. He has taught me invaluable lessons and provided numerous opportunities that I am truly grateful for. His understanding, patience, and vast knowledge have shown me the kind of person and professional I aspire to become. Professor, thank you for everything. It has been an absolute honor to be one of your students.

This dissertation was written in LaTeX according to the IAGTESE template, for thesis and dissertations of the Institute of Astronomy, Geophysics and Atmospheric Sciences.

Abstract

This work explores deriving splashback radii (R_{sb}) solely from SDSS (Sloan Digital Sky Survey) photometric data and their correlation with M_{200} masses from weak-lensing analyses. Our analysis indicates splashback radii preferences around $R_{sb}/R_{200} \approx 0.45$ and $R_{sb}/R_{200} \approx 0.7$, revealing distinct populations based on cluster concentration. We establish a strong correlation between splashback radii and cluster masses with a dispersion of 0.19 dex. Future work involves exploring the bimodal nature of splashback radii and proposing an intuitive method, estimating the splashback mass for a more representative cluster mass. We show the feasibility of deriving splashback radii and cluster masses using photometry, offering potential advancements in observational cosmology.

Resumo

Este trabalho explora a obtenção de raios de *splashback* (R_{sb}) exclusivamente a partir de dados fotométricos do SDSS (Sloan Digital Sky Survey) e sua correlação com massas M_{200} derivadas de análises de lente fraca. Nossa análise indica preferências de raios de *splashback* em torno de $R_{sb}/R_{200} \approx 0.45$ e $R_{sb}/R_{200} \approx 0.7$, revelando populações distintas com base na concentração do aglomerado. Estabelecemos uma forte correlação entre os raios de *splashback* e as massas dos aglomerados com uma dispersão de 0.19 dex. Trabalhos futuros envolvem explorar a natureza bimodal dos raios de *splashback* e propor um método intuitivo, estimando a massa de *splashback* para uma medida mais representativa. Este estudo demonstra a viabilidade de derivar raios de *splashback* e massas de aglomerados usando fotometria, oferecendo possíveis avanços na cosmologia observacional.

Contents

Chapter 1

Introduction

Galaxy clusters are the largest bound structures observed in the universe and provide crucial insights into the formation and evolution of cosmic structures. Due to their nature, galaxy clusters serve as valuable laboratories for testing and advancing our understanding of cosmology, galaxies and large scale structure evolution.

The study of cluster evolution across cosmic time is closely tied to various cosmological parameters, including the growth rates of primordial density fluctuations, as well as the cosmic volume-redshift relation. These close relations arise because galaxy cluster halos occupy the exponential tail of the cosmic mass function (e.g., Haiman et al. 2001). Consequently, by measuring a large number of galaxy clusters spanning a wide range of masses and redshifts, we can place strong constraints on cosmological models (e.g., Allen et al. 2004; Vikhlinin et al. 2009; Pratt et al. 2019).

However, accurate mass estimations of galaxy clusters typically require expensive instrumentation or complex methods such as spectroscopic measurements using the Virial Theorem (e.g., Carlberg et al. 1997), X-ray observations with scale relations (e.g., Arnaud et al. 2005), or weak-lensing analyses, which can introduce significant biases and systematic errors if not carefully performed (Umetsu et al., 2020a). Moreover, with the advent of new photometric surveys such as the Southern Photometric Local Universe Survey (S-PLUS; Mendes de Oliveira et al. 2019), the Javalambre Photometric Local Universe Survey (J-PLUS; Cenarro et al. 2019), and the Javalambre-Physics of the Accelerating Universe Astrophysical Survey (J-PAS; Bonoli et al. 2021), there is a need for novel techniques to measure cluster masses using the vast amount of photometric data available.

In addition to mass, the study of galaxy clusters encompasses other important features. Specifically, Fillmore and Goldreich (1984) and Bertschinger (1985) demonstrated that

models of self-similar secondary infall of matter onto a spherical overdensity predict a density jump at the location where recently infalling material reaches its first apocenter, corresponding to the last density caustic. This location is referred to as the splashback radius (R_{sb}), which serves as a significant tracer of a cluster's history. The splashback radius is closely linked to mass accretion rates and can delineate the boundary between the virialized region and the surroundings where particles are falling into the cluster for the first time. Furthermore, the R_{sb} plays an intriguing role in the study of galaxy evolution, as galaxies within this region have already passed through the cluster center, resulting in modifications to their color and stellar population.

Adhikari et al. (2021) further explored the relationship between galaxy colors and the splashback radius. They found that galaxies of different colors exhibit different R_{sb} locations, which can be interpreted as the average time of infall for each population. Notably, blue galaxies tend to be the most recently accreted and have not yet reached their apocenter. This color-dependent mapping provides insights into the timing and process of galaxy infall and can shed light on the connection between galaxy properties and their environment within clusters.

The splashback radius was initially derived from simulations (Diemer and Kravtsov 2014; Adhikari et al. 2014; More et al. 2015) and the first observational evidence was presented by More et al. (2016, hereafter referred to as More16). More16 utilized the surface number density profile of clusters and identified the steepest slope as an indicator of the density jump associated with the splashback radius. More recently, Kopylova and Kopylov (2023, referred to as K&K; see also Kopylova and Kopylov 2018 and Kopylova and Kopylov 2019) introduced a simpler and more robust method for estimating the splashback radius. K&K's method is based on the cluster's cumulative distribution, providing a practical approach to determining R_{sb}. Notably, both methods depend only on photometric data.

The objective of this study is to assess the reliability of R_{sb} estimates obtained from photometric data. Additionally, we aim to establish a scale relation between cluster masses and the splashback radius, enabling us to evaluate masses using solely photometric information.

To achieve this, we merged data from the Sloan Digital Sky Survey (SDSS) DR16[1], combining methodologies proposed by More16 and K&K. This approach integrates the

[1] https://skyserver.sdss.org/dr16/en/tools/search/sql.aspx

robust cumulative data from K&K while incorporating the physical insights derived from More16's modeling. Although this work is preliminary, it has yielded intriguing results, aligning with findings confirmed by other researchers, especially in distinct cluster populations.

Throughout the work, we adopt a flat ΛCDM cosmology with parameters $\Omega_M = 0.28$ and $\Omega_\Lambda = 0.72$, and a Hubble constant of $H_0 = 100h$ kms^{-1}Mpc^{-1}, with $h = 0.7$. We employ the standard notation M_Δ to represent the mass enclosed within a sphere of radius R_Δ, where the mean overdensity equals $\Delta \times \rho_c(z)$, with ρ_c denoting the critical closure density of the universe.

Chapter 2

Data

In this chapter, we provide details on the data used in our analysis for mass fitting calibrations using weak-lensing information.

2.1 Weak-lensing information

For the mass calibration, we utilized publicly available data from Umetsu et al. (2020b). They conducted a weak-lensing analysis of X-ray galaxy clusters selected from the XMM-XXL survey (Pierre et al., 2016). Optical images from the Hyper Suprime-Cam Subaru Strategic Program (Aihara et al., 2017, 2018) were used for the analysis. The dataset consisted of 136 spectroscopically confirmed galaxy clusters in the redshift range of $0.031 < z < 1.033$. The weak-lensing analysis provided estimates of M_{200} mass and concentration parameter (c) by fitting a spherical NFW density profile (Navarro et al., 1996, 1997). The mass estimates were bias-corrected based on the clusters' X-ray temperature, which was also provided in the data (see Umetsu et al. 2020b for detailed methodology). Additionally, we used mass data from Kiiveri et al. (2021), which performed a weak-lensing analysis on 25 galaxy clusters from the COnstrain Dark Energy with X-ray (CODEX) sample. These clusters were selected based on a 4σ photon excess from the ROSAT All-Sky Survey (RASS) (Voges et al., 1999). The analysis utilized X-ray information and optical images from the Mega-Cam (Boulade et al., 2003) at the Canada-France-Hawaii Telescope. The masses were estimated using a Bayesian hierarchical scheme for combined likelihoods, assuming, once more, an NFW density profile (full details in Kiiveri et al. 2021).

2.2 Redshift information and cluster selection

For cluster selection, our primary focus was on accurately estimating cluster parameters through photometry. As a result, we adopted selection criteria that prioritize robust photometric redshift (photo-z) estimation. To achieve this, we leveraged data from the Sloan Digital Sky Survey (SDSS), given that a substantial portion of our cluster samples resided within the survey footprint. The SDSS not only covers this area comprehensively but also exhibits high-quality fine-tuning in photo-z estimation, boasting a typical error of $\sigma_0 = 0.0205$ (for methodologies from DR10 and subsequent releases, refer to Beck et al. 2016).

In our selection process, we exclusively included galaxies flagged as *CLEAN*, a designation that ensures exclusion of data from saturated, deblended, and masked areas within SDSS images. Additionally, we applied corrections to magnitudes to account for galactic dust extinction.

It is important to note that due to the prevalence of high-redshift weak-lensing samples, where SDSS observation coverage of cluster members is limited, our selection criteria resulted in a constrained number of identified clusters. Specifically, we identified 12 galaxy clusters within the XMM-XXL survey (referred to as the XXL sample) and 11 clusters within the CODEX sample.

Chapter 3

Methods

3.1 Probabilistic cluster membership

In our pursuit of estimating splashback radii, we aimed to compare outcomes employing a basic $3\sigma_0$ criterion for cluster membership against a probabilistic approach offering a more robust definition of cluster members. The objective was to evaluate the impact of field galaxies on our results.

Expanding upon the methodology introduced by Castignani and Benoist (2016), this study reproduced the estimation of a galaxy's likelihood to belong to a specific group or cluster, considering criteria such as the surplus of galaxies within redshift bins, magnitude, and the solid angle between the cluster and its surrounding field.

By leveraging Bayes' Theorem and assuming normal distributions for both spectroscopic redshift (z_s) and photometric redshift (z_p), the probability of a galaxy g having its spec-z within a certain interval given its photo-z is calculated as:

$$P(z_{s,g}|z_{p,g}) \propto \mathcal{N}(z_s) \cdot \mathcal{N}(z_{p,g}, \mu = z_{s,g}, \sigma = \sigma_0(1 + z_{s,g})), \tag{3.1}$$

where, σ_0 represents the typical error in photo-z, approximately $\simeq 0.02$ in our analysis.

To prevent introducing bias, the spec-z distribution is considered constant, leading to a simplified expression:

$$P_g(z) \propto \frac{1}{\sigma_0(1 + z_{s,g})} \exp\left[-\frac{(z - z_{p,g})^2}{2\sigma_0^2(1 + z_{s,g})^2}\right]. \tag{3.2}$$

Normal distributions are also assumed for the group/cluster c and galaxy magnitude m:

$$P_c(z) = \mathcal{N}(z, \mu = z_c, \sigma = \sigma_0(1 + z_c)), \tag{3.3}$$

$$P_g(m) = \mathcal{N}(m, \mu = m_g, \sigma = \delta m), \tag{3.4}$$

where δm signifies the expected statistical error in photometry, approximately $\simeq 0.1$.

The field density, termed N_{glob}, outside the cluster is defined as:

$$N_{glob}(m, z) = \frac{1}{\Omega} \sum_g P_g(z) P_g(m), \tag{3.5}$$

where, Ω denotes a survey field's area of approximately 10 sq. deg., effectively capturing small-scale features within our clusters.

To prevent very low counts, the mean field density $< N_{glob}(m, z) >$ is calculated using:

$$< N_{glob}(m, z) >= \int_{m-5\delta_m}^{m+5\delta_m} \int_{z-2\sigma_0(1+z_c)}^{z+2\sigma_0(1+z_c)} N_{glob}(m', z') dz' dm'. \tag{3.6}$$

Similarly, the mean local density N_{loc} within the cluster accounts for counts in a ring between $r - dr$ and $r + dr$, relating to the galaxy's position r from the center:

$$N_{loc}(m, z, r) = \frac{1}{d\Omega} \sum_g P_g(z) P_g(m), \tag{3.7}$$

where $d\Omega$ defines an area equal to a circle of radius 0.45 Mpc, typical for cluster central parts.

After the technical steps outlined in detail in Castignani and Benoist 2016, Bayesian inference allows us to ascertain the probability of a galaxy g belonging to group/cluster c given Photo-z, magnitude, and distance to the center:

$$\mathcal{P}(g \in c | z_p, m, r) \simeq (1 - \beta)\delta z \int P_g(z) P_z(z) dz \simeq (1 - \beta) \sum_i P_g(z_i) P_c(z_i), \tag{3.8}$$

where $\beta = \frac{<N_{glob}(m_g, z_c)>}{<N_{loc}(m_g, z_c, r_g)>}$ and δz represents the chosen redshift bin size, 0.01 in our analysis.

This probability is relative and unnormalized. To constrain values between 0 and 1, the maximum probability is estimated when $\beta << 1$. Consequently, the final absolute expression is obtained as:

$$P_{mem} = \frac{(1-\beta)\sum_i P_g(z_i)P_c(z_i)}{0.047\left(\frac{\delta z}{0.01}\right)\left(\frac{1+z_c}{2}\right)^{-1}\left(\frac{\sigma_0}{0.03}\right)^{-1}}, \tag{3.9}$$

where all Probability Density Functions (PDFs) are assumed to be normalized.

3.2 Cumulative profile model

As demonstrated in simulations by More et al. (2015), approximating the splashback radius involves identifying the radius exhibiting the steepest logarithmic slope, prompting considerable interest in observing this phenomenon in real data. However, attempting a direct determination from observational data often introduces significant noise and bias. Hence, many researchers have resorted to modeling the surface number density of galaxy clusters and inferring R_{sb} from the fitted profile.

Our approach integrates the model analysis proposed by More16 with the recently introduced cumulative profile from K&K. Modeling the cumulative profile instead of the surface number density offers an advantage: cumulative distributions are less susceptible to statistical fluctuations compared to surface number density. Consequently, we devised a composite of two halo models from Diemer (2023) within a projected sum involving a truncated Sérsic profile and a modified long 2-halo term:

$$\Sigma_{sersic}(R) = \Sigma_0 \exp\left(-\left(\frac{R}{R_s}\right)^{\frac{1}{n}} - \left(\frac{R}{R_t}\right)^{\frac{1}{m}}\right), \tag{3.10}$$

$$\Sigma_{2-halo}(R) = \Sigma_m \left[\frac{1}{\sqrt{(1/d_{\max})^2 + \left(\frac{R}{R_t}\right)^{2\gamma}}} + 1\right], \tag{3.11}$$

where, Σ_0 represents the point zero density, R_s is the common scale radius, R_t signifies the truncation radius where the Sérsic profile begins sharpening, and n and m denote the steepening and sharpening parameters, respectively. Additionally, Σ_m stands for the mean density of the universe, $d_{\max}$ serves as a normalization factor preventing dominance of the 2-halo term in central regions, and γ represents the slope of the 2-halo term.

Utilizing this formulation, the cumulative profile is derived as:

$$N(< R) = \int_0^R 2\pi R\Sigma(R)dR, \tag{3.12}$$

where N represents the number of galaxies within projected clustercentric radius R, and $\Sigma(R)$ combines $\Sigma_{sersic}(R)$ and $\Sigma_{2-halo}(R)$.

To sample from the posterior distribution detailed in Table 3.1, we employed the affine invariant Markov Chain Monte Carlo (MCMC) sampler developed by Goodman and Weare (2010). Notably, significant parameter degeneracy between Σ_0 and R_s led us to derive the zero-point density estimation directly from the data. Precisely, we calculated the surface number density within a radius of 0.1 Mpc from the center and employed it as a prior within the method.

Owing to the diverse range of clusters observed across varying redshifts, our modeling strategy implemented an absolute magnitude limit of $M_r < -19.5$. This threshold corresponds to an estimated magnitude of $m_r \approx 21$ at our mean redshift of 0.3. Additionally, our modeling procedures were constrained within a maximum cluster-centric distance of 5 Mpc. This restriction was chosen purposefully to align with the scales relevant to our investigation, considering that the splashback radius is expected to be in the vicinity of R_{200}.

Table 3.1 - Model parameter priors. In case of fixed or gaussian priors, the reference is given.

Parameter	Prior	Value	Reference
Σ_0	fixed	estimated from data	-
R_s	flat	0.1, 2	-
R_t	flat	0.25, 2.5	-
n	fixed	2.4	Beraldo e Silva et al. (2013)
m	fixed	0.35	Diemer (2023)
Σ_m	flat	0, 10^2	-
$d_{\max}$	fixed	1	Bianconi et al. (2021)
γ	gaussian	0.8 ± 0.25	Wang et al. (2013)

Chapter 4

Results

4.1 Probabilistic membership tests

To validate the robustness of our method and gain comprehensive insights into its performance under varying member probability thresholds, we applied our algorithm to a galaxy mock dataset provided by Pablo Araya-Araya, a collaborator within our research group. This mock dataset, constructed based on S-PLUS data, serves as an effective environment to thoroughly test our analysis, mimicking real scenarios.

We specifically selected galaxy clusters within the range of $14 < \log(M_{200}/M_{\odot}) < 15$ and $0.01 < z < 0.6$, ensuring a representative sample akin to our actual data. The analysis was performed within the cluster's R_{200} region.

For each cluster, we identified several categories: $N_{\text{estimated}}$, representing the number of galaxies classified as cluster members based on our membership assignments; N_{true}, denoting the count of actual true cluster members; $N_{\text{interlopers}}$, signifying sources mistakenly identified as cluster members; and N_{missed}, indicating true cluster members not identified.

In Figure 4.2, we present a stacked histogram illustrating all mock clusters. The blue bars depict interloper galaxies, while the pink bars represent true members. Additionally, Figure 4.2 displays a ROC curve, delineating the trade-off between purity (p) and completeness (c), defined as (George et al., 2011):

$$p = 1 - \frac{N_{\text{interlopers}}}{N_{\text{estimated}}}, \tag{4.1}$$

$$c = 1 - \frac{N_{\text{missed}}}{N_{\text{true}}}. \tag{4.2}$$

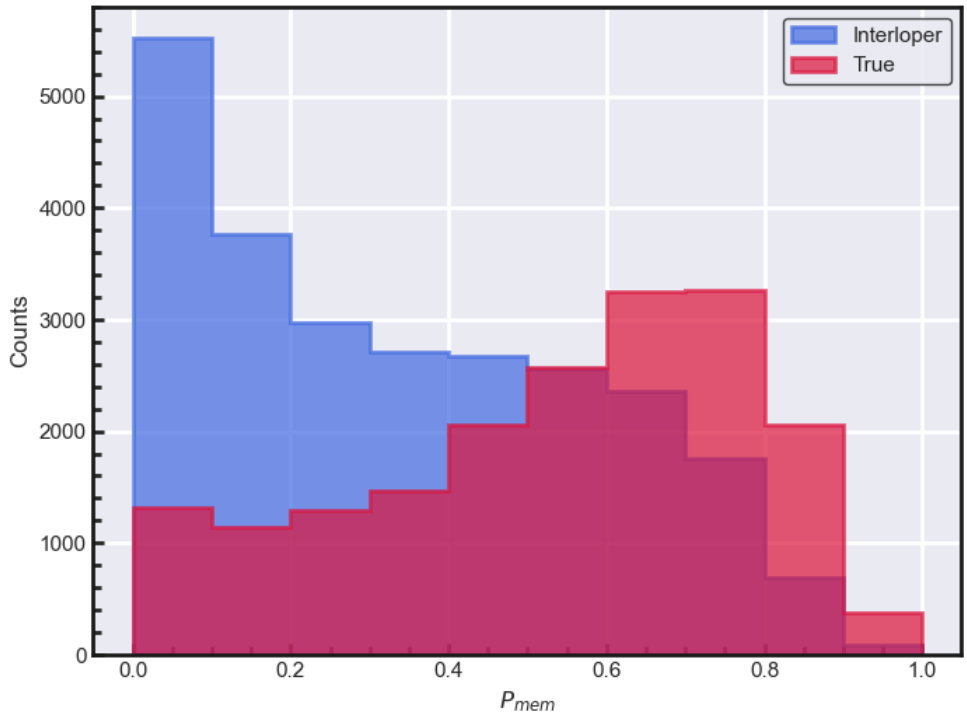

Figure 4.1: Stacked histogram of mock galaxy clusters. In blue, interloper galaxies, in pink, real members.

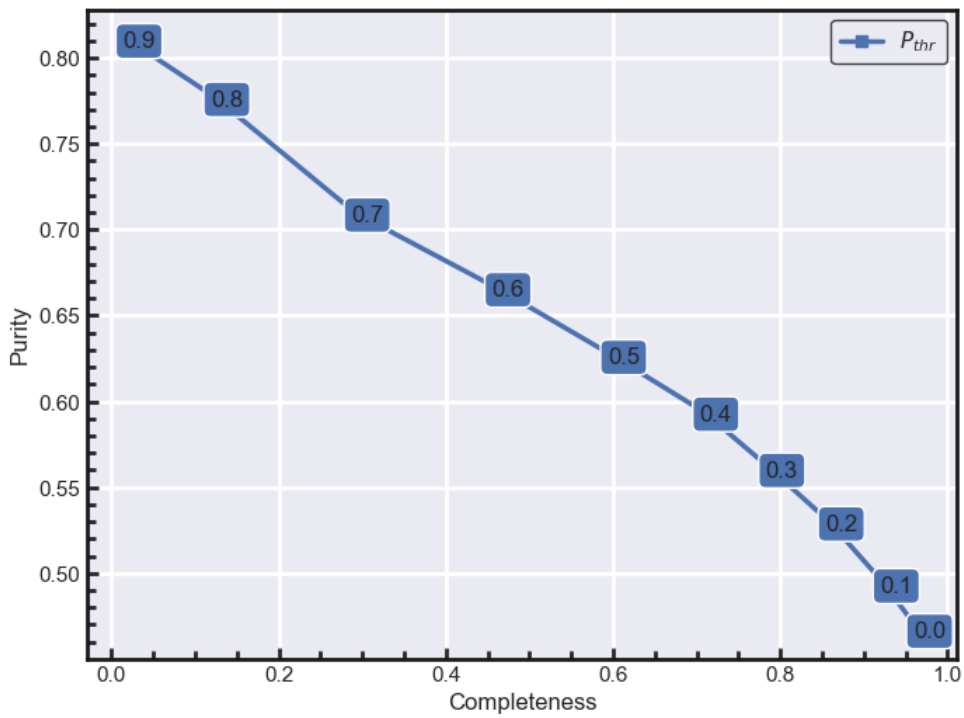

Figure 4.2: Purity vs. completeness of mock galaxy clusters membership.$P_{\rm thr}$ indicates the membership probability threshold

Based on these results, we made the intuitive decision to classify galaxies as members if their membership probability exceeds a probability threshold ($P_{\rm thr}$) of 0.5. This choice yields a purity and completeness rate exceeding 60%, demonstrating favorable values given the inherent uncertainties in photo-z membership estimation.

Additionally, we calculated a derived quantity, denoted as $R_{\rm mem}$, representing the weighted mean distance of galaxies within each cluster from its center. This mean distance is determined by considering the member probability associated with each galaxy. In our analysis, we specifically focused on galaxies with a member probability exceeding 0.5 and located within $1h^{-1}$Mpc from the cluster center. Notably, this metric has been suggested as a potential proxy for gauging the cluster concentration, as discussed in More16. In Figure 4.3, the distribution of $R_{\rm mem}$ for our samples reveals intriguing patterns, notably showing two distinct populations at approximately $R_{\rm mem} \approx 0.34h^{-1}$Mpc and $R_{\rm mem} \approx 0.46h^{-1}$Mpc. Further discussion regarding this observation is detailed in the subsequent section.

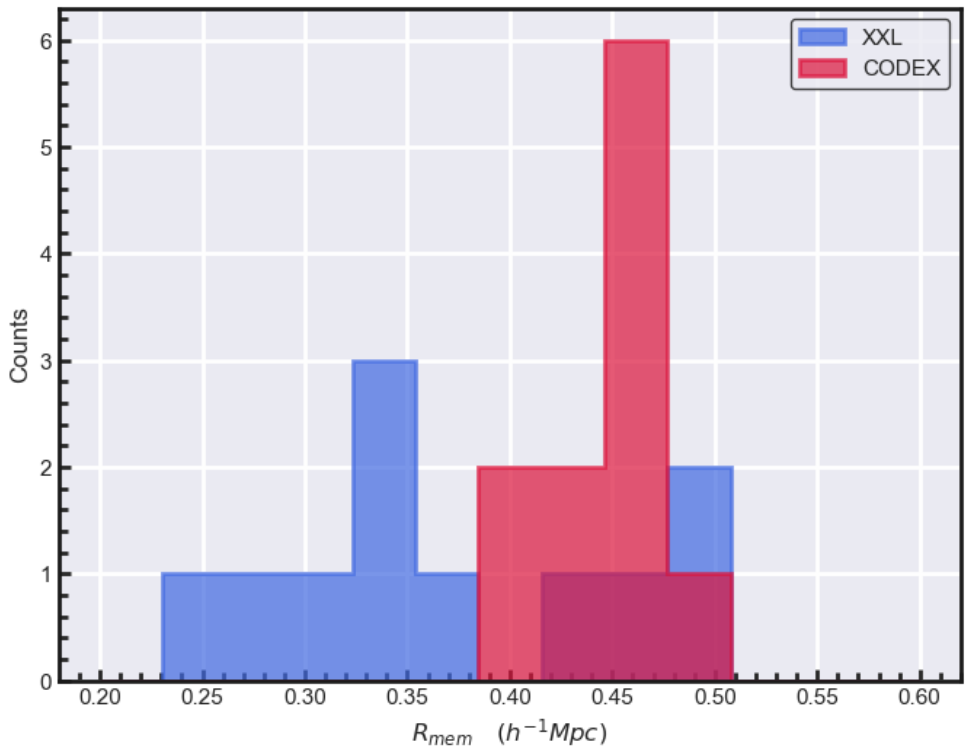

Figure 4.3: Weighted mean distance of galaxies from its cluster center.

4.2 Splashback radius estimation

4.2.1 Basic σ_0 cut

For our initial analysis, we opted to define cluster membership by selecting galaxies with a photo-z falling within a $3 \times (1+z)\sigma_0$ cut from the redshift cluster center. This choice, though more conservative, ensures the inclusion of the majority of galaxy members within the magnitude limit. However, it also introduces a potential for significant contamination from field galaxies due to the larger order of magnitude of photo-z compared to the expected velocity dispersion for typical clusters.

We proceeded with modeling each cluster within our samples, deriving the steepest logarithmic slope of the density profile from the obtained parameter posteriors, yielding a distribution for R_{sb}. In Figure 4.4, we present an illustrative instance displaying the parameter posteriors and the fitted profile for a cluster within the CODEX sample, yielding an obtained value of $R_{sb} = 1.13 \pm 0.12 h^{-1}$Mpc. Additionally, Figure 4.5 showcases the distribution of splashback radii across our samples.

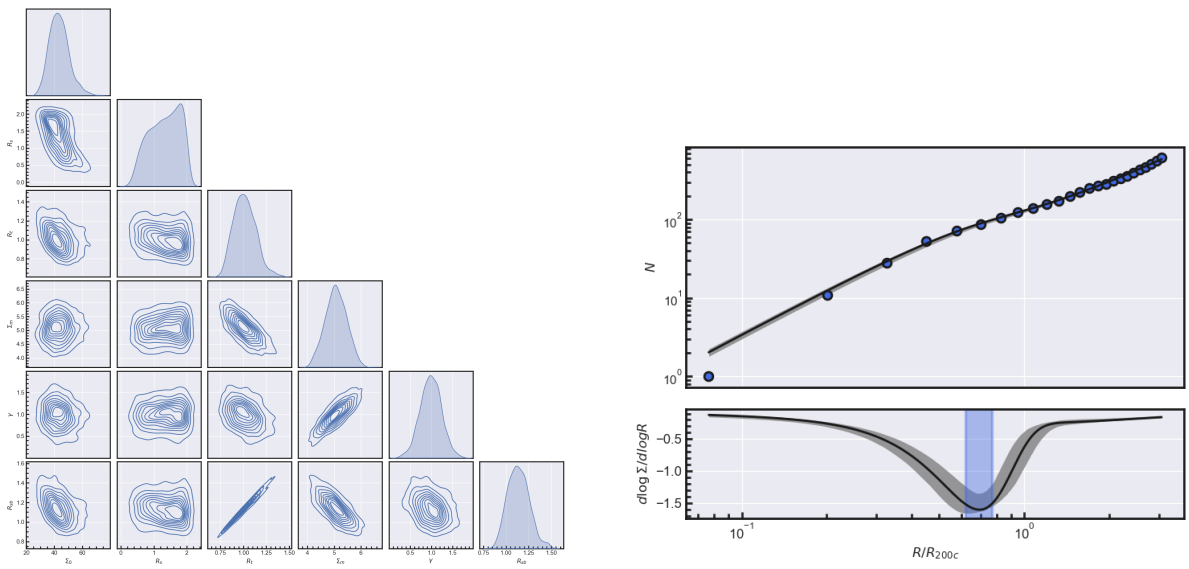

(a) Parameter posteriors. (b) Fitted profile.

Figure 4.4: Example of profile modeling for cluster 24872 from CODEX sample.

An intriguing observation emerges from Figure 4.6: the ratio R_{sb}/R_{200c}, with R_{200c} denoting the cluster's R_{200} concerning the critical density of the universe, exhibits bimodality akin to the observed bimodality in the R_{mem} distribution. This phenomenon was previously documented in More16, where splashback radii were observed to prefer locations around

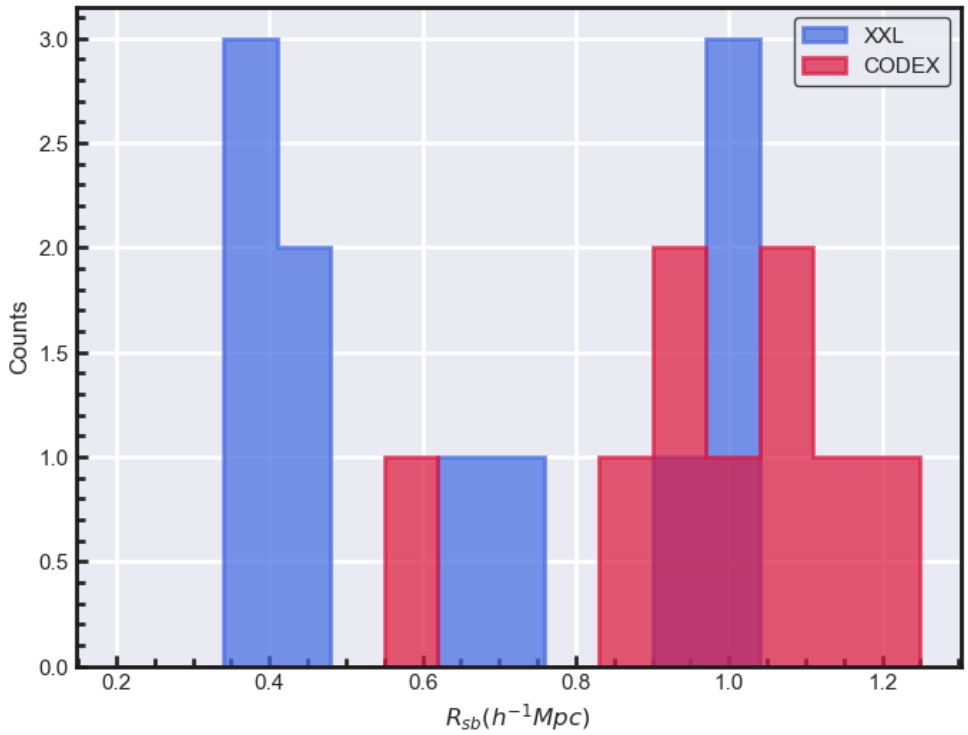

Figure 4.5: Splashback radius distribution for CODEX and XXL samples.

$R_{sb}/R_{200m} \approx 0.67$ and $R_{sb}/R_{200m} \approx 0.95$, considering R_{200m} as the cluster's R_{200} concerning the mean density of the universe. In our study, we observe values of $R_{sb}/R_{200c} \approx 0.45$ and $R_{sb}/R_{200c} \approx 0.7$, aligning reasonably well with More16's findings, considering that different R_{200} are expected to exist at distinct locations varying with redshift.

This bimodality in the R_{sb}/R_{200} ratio might be influenced by various cluster properties, including the accretion rate (Diemer and Kravtsov, 2014) and particularly the cluster concentration. Leveraging the R_{mem} of each cluster, we segregated the two populations using a visual cut at $R_{mem} < 0.4$ for higher concentrations (hereafter labeled the c_{high} population) and $R_{mem} > 2.8$ for lower concentrations (hereafter labeled the c_{low} population). Figure 4.7 illustrates the behavior of these two populations in the ratio space. Ultimately, our mass fitting in Figure 4.8 reveals the total fitting with a dispersion of ≈ 0.19 dex and the fitting accounting for the bimodality, showcasing a dispersion of ≈ 0.15 dex in both scenarios. Both choices exhibit robust visual correlations and contribute significantly to our primary goal of estimating photometric masses.

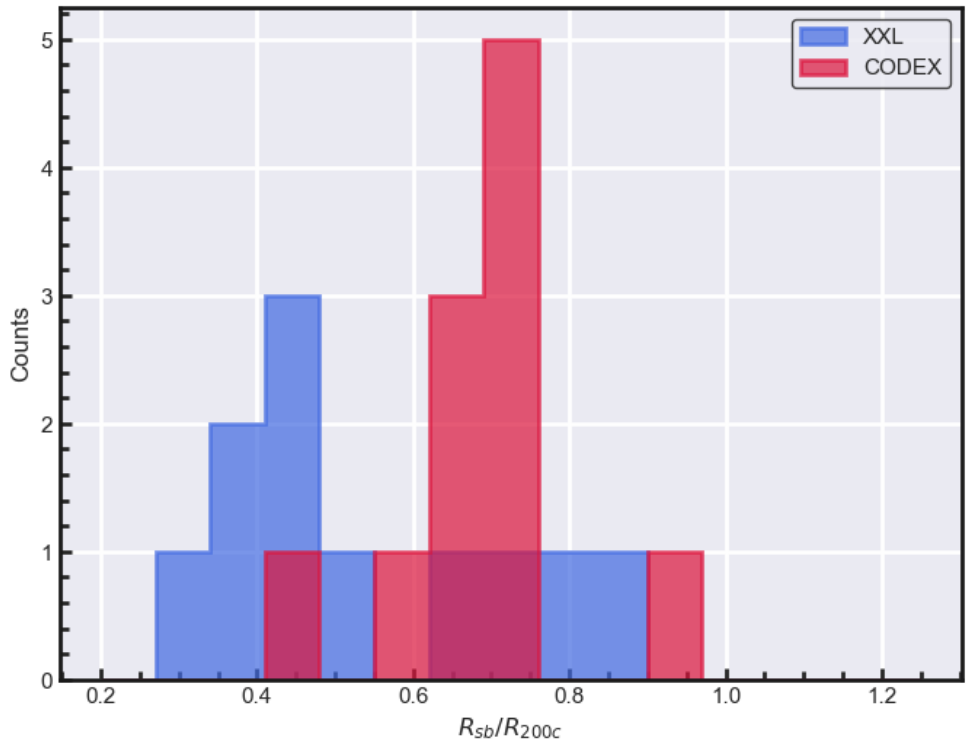

Figure 4.6: Ratio R_{sb}/R_{200c} for CODEX and XXL samples. The data suggests the presence of distinct populations.

4.2.2 Probability membership

Although our model predicts a contribution from field galaxies, employing a simple photo-z cut significantly diminishes the signal-to-noise ratio. This reduction makes it challenging to distinguish clusters from the mean density field, especially evident in smaller systems such as groups and poor clusters. Hence, we made the decision to conduct an additional modeling approach based on the cumulative profile, considering only galaxies with a member probability higher than 50% as described in Section 4.1. While this method leads to a loss of some galaxies, it offers a more insightful understanding of the core aspects of the cluster. Furthermore, it enables comparisons between modeling outcomes using solely the σ_0 criteria.

In Figure 4.9, we present an example for the same cluster (24872 from CODEX sample) as discussed in the previous section, showcasing the parameter posterior distributions and the fitted profile. Despite observed parameter differences, the splashback radius remains consistent, accounting for statistical fluctuations, with a measured value of $R_{sb} = 1.35 \pm 0.12h^{-1}$Mpc.

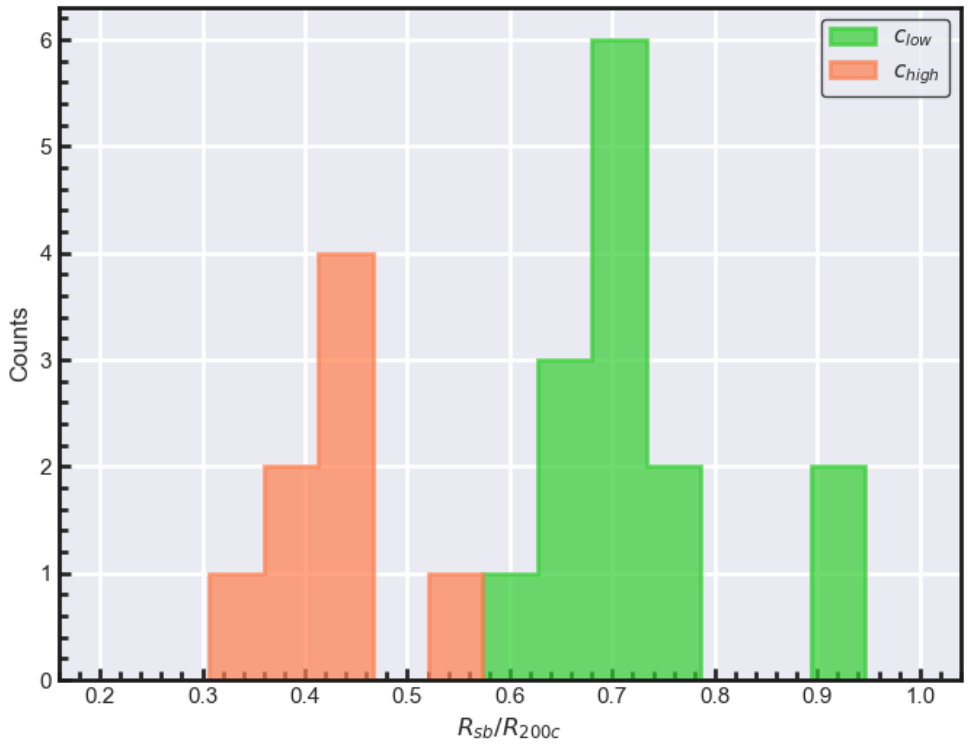

Figure 4.7: Ratio R_{sb}/R_{200c} revealing the potential of concentration in distinguishing each population.

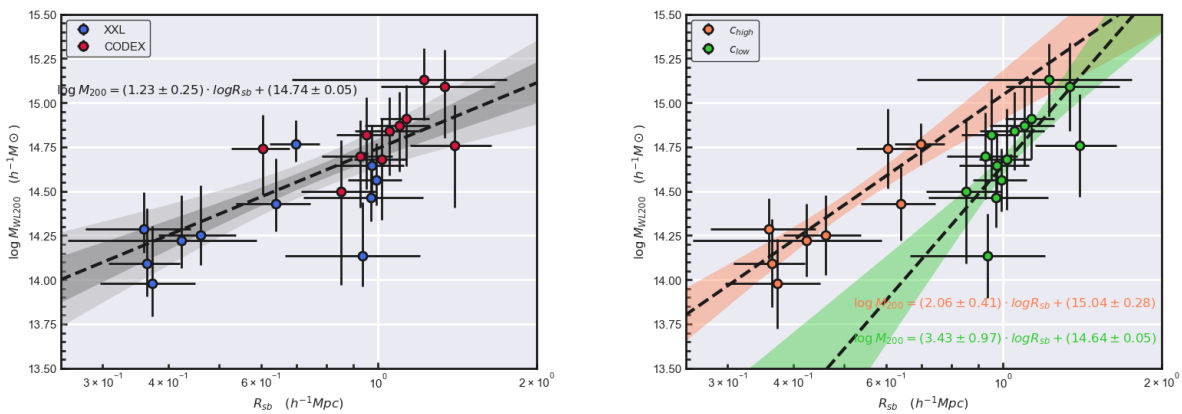

(a) Total. (b) Bimodality.

Figure 4.8: Mass fittings between M_{200} and R_{sb}. The dispersions found are ≈ 0.19 for the total and ≈ 0.15 for both bimodal populations.

Additionally, for a comprehensive comparison, Figure 4.10 illustrates the R_{sb} values obtained in both scenarios-the member probability and the photo-z cut. Despite the presence of high noise, the observed values appear consistent, lacking any discernible structure, with a mean ratio of $R_{sb-\text{member prob}}/R_{sb-\sigma_0 \text{ cut}} = 1.3 \pm 0.3$, consistently hovering around 1. The

relatively higher values in the member probability case can be attributed to the significant reduction in field contamination. In some instances, this reduction can lead to mean density approaching 0, an unexpected outcome in our model.

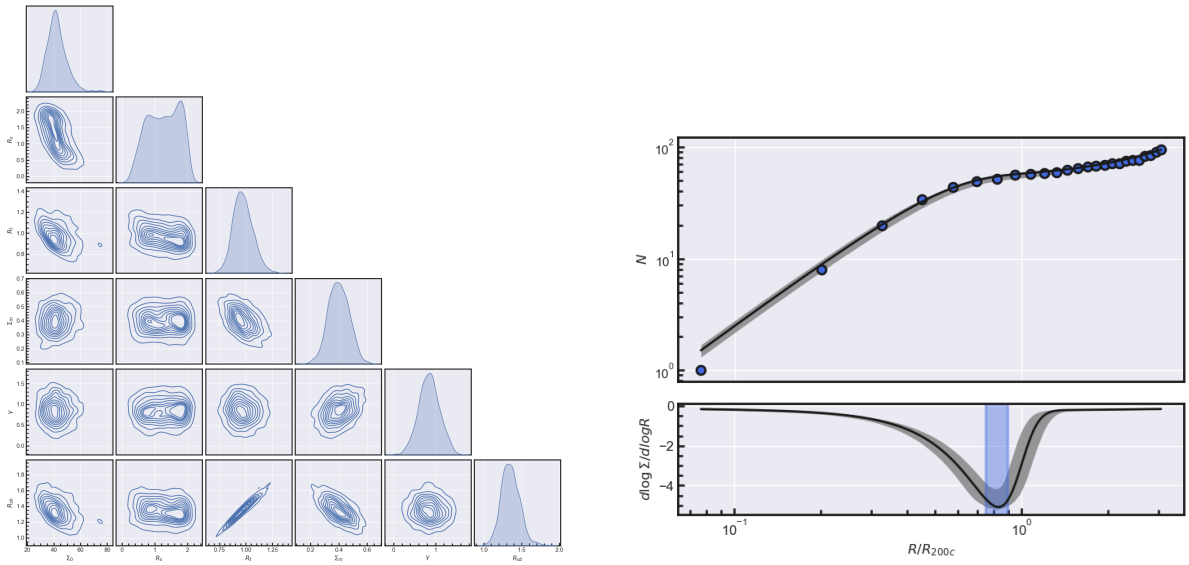

(a) Parameter posteriors. (b) Fitted profile.

Figure 4.9: Example of profile modeling for cluster 24872 from CODEX sample.

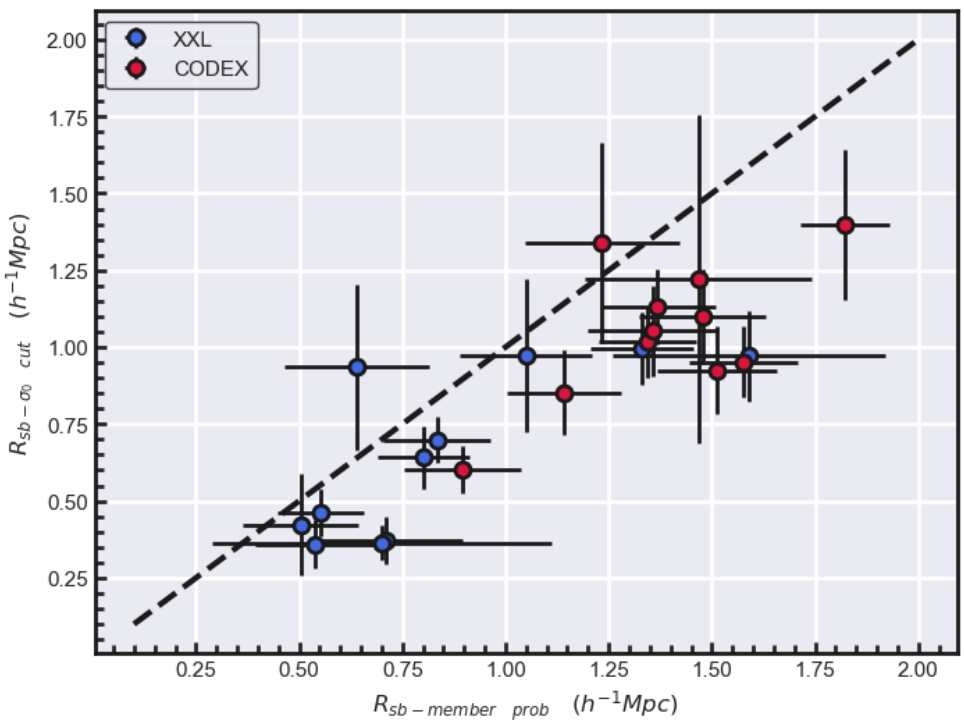

Figure 4.10: Comparison between splashback radius estimations in cases basic σ_0 criteria and membership probability, with a mean ratio of $R_{sb-\text{member prob}}/R_{sb-\sigma_0\text{ cut}} = 1.3 \pm 0.3$.

Figure 4.11 showcases the total mass fitting in the current scenario, revealing no discernible improvement, with a dispersion of ≈ 0.2. Consequently, we contend that employing membership probability, besides being an additional step in the analysis, it also relies heavily on survey-specific properties such as typical errors in photo-z, magnitude limits, completeness, and more. As we aim to apply our method across various photometric surveys, we assert that the optimal choice remains the basic photo-z cut.

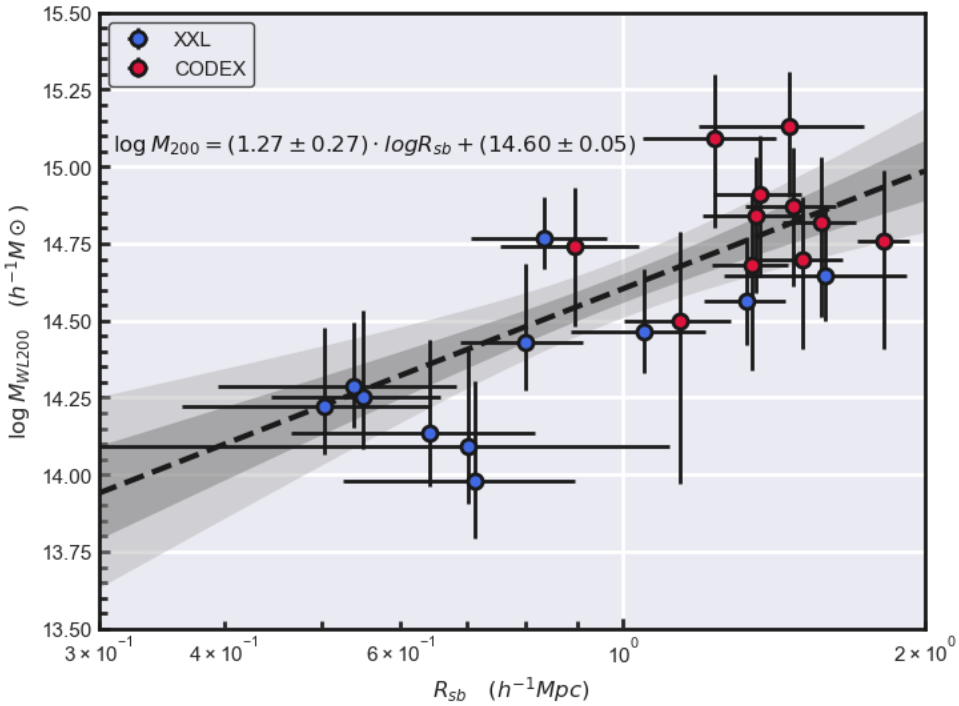

Figure 4.11: Mass fittings between M_{200} and R_{sb} for the member probability case.

Chapter 5

Conclusion

This study conducted an in-depth analysis of splashback radius estimations modeling the cumulative distribution of SDSS photometric clusters. The primary aim was twofold: to ascertain the feasibility of evaluating R_{sb} solely using photometric data and to establish a relationship between photometric splashback radii and M_{200} masses derived from weak-lensing analyses (see Sections 2 and 3).

An intermediate step involved reproducing the cluster membership probability estimations from Castignani and Benoist (2016), yielding consistent results in terms of system purity and completeness. Using an intuitive membership probability cut of 0.5, we achieved completeness and purity levels exceeding 60% (see Section 4.1).

Our findings regarding splashback radius estimations suggest a preference for locations around $R_{sb}/R_{200} \approx 0.45$ and $R_{sb}/R_{200} \approx 0.7$, with these two distinct populations easily distinguishable using a concentration-based criterion. Moreover, a robust correlation between splashback radii and cluster masses was observed, displaying a total dispersion of 0.19 dex (see Section 4.2.1).

In the modeling of clusters considering membership probability, while maintaining consistent R_{sb} estimations, no discernible improvements were noted, and greater dispersions were observed in mass fittings. Therefore, we advocate for the use of the basic photo-z cut as the optimal approach (see Section 4.2.2).

In future investigations, exploring and understanding the bimodal nature of splashback radii findings could be insightful. However, this bimodality poses challenges in mass fittings, especially when avoiding membership probability analysis, complicating the separation based on concentration. To address this, we propose a more intuitive approach: estimating the splashback mass, derived from the mass enclosed within a sphere of radius

R_{sb}. This method avoids dealing with different populations and, given that the splashback radius signifies a physical limit for the cluster halo, provides a more representative cluster mass.

Future endeavors aim to validate these findings across various photometric surveys, enabling extensive mass estimations across different redshifts, an ideal scenario to study the cosmological mass distribution of clusters. Additionally, investigating galaxy properties and evolution around the splashback radius is planned, considering that most galaxies in this region likely passed through the cluster center, potentially resulting in significant effects on their stellar populations.

In summary, our results demonstrate the feasibility of estimating splashback radii using photometry and deriving cluster masses with good precision. This breakthrough holds promise in observational cosmology, paving the way for a deeper comprehension of galaxy cluster nature.

Bibliography

Adhikari S., et al., Splashback in accreting dark matter halos, Journal of Cosmology and Astroparticle Physics, 2014, vol. 2014, p. 019

Adhikari S., et al., Probing Galaxy Evolution in Massive Clusters Using ACT and DES: Splashback as a Cosmic Clock, The Astrophysical Journal, 2021, vol. 923, p. 37

Aihara H., Arimoto N., Armstrong R., et al., The Hyper Suprime-Cam SSP Survey: Overview and survey design, Publications of the Astronomical Society of Japan, 2017, vol. 70

Aihara H., Arimoto N., Armstrong R., et al., First data release of the Hyper Suprime-Cam Subaru Strategic Program, Publications of the Astronomical Society of Japan, 2018, vol. 70

Allen S. W., et al., Constraints on dark energy from Chandra observations of the largest relaxed galaxy clusters, Monthly Notices of the Royal Astronomical Society, 2004, vol. 353, p. 457

Arnaud M., et al., The structural and scaling properties of nearby galaxy clusters II. The M-T relation, Astronomy & Astrophysics, 2005, vol. 441, p. 893

Beck R., Dobos L., Budavári T., Szalay A. S., Csabai I., Photometric redshifts for the SDSS Data Release 12, Monthly Notices of the Royal Astronomical Society, 2016, vol. 460, p. 1371

Beraldo e Silva L. J., et al., Testing phenomenological and theoretical models of dark matter density profiles with galaxy clusters, Monthly Notices of the Royal Astronomical Society, 2013, vol. 000, p. 1

Bertschinger E., Self-similar secondary infall and accretion in an Einstein-de Sitter universe, Astrophysical Journal Supplement Series, 1985, vol. 58, p. 39

Bianconi M., et al., LoCuSS: The Splashback Radius of Massive Galaxy Clusters and Its Dependence on Cluster Merger History, The Astrophysical Journal, 2021, vol. 911, p. 2

Bonoli S., et al., The miniJPAS survey: A preview of the Universe in 56 colors, Astronomy & Astrophysics, 2021, vol. 653, p. A31

Boulade O., et al., Instrument Design and Performance for Optical/Infrared Ground-based Telescopes, SPIE, 2003, vol. 4841, p. 72

Carlberg G. R., et al., The Average Mass and Light Profiles of Galaxy Clusters, The Astrophysical Journal, 1997, vol. 478, p. 462

Castignani G., Benoist C., A new method to assign galaxy cluster membership using photometric redshifts, Astronomy & Astrophysics, 2016, vol. 595, p. A111

Cenarro A. J., et al., J-PLUS: The Javalambre Photometric Local Universe Survey, Astronomy & Astrophysics, 2019, vol. 622, p. A176

Diemer B., A dynamics-based density profile for dark haloes - II. Fitting function, Monthly Notices of the Royal Astronomical Society, 2023, vol. 519, p. 3292

Diemer B., Kravtsov A. V., Dependence of the Outer Density Profiles of Halos on Their Mass Accretion Rate, The Astrophysical Journal, 2014, vol. 789, p. 1

Fillmore J. A., Goldreich P., Self-similar gravitational collapse in an expanding universe, Astrophysical Journal, 1984, vol. 281, p. 1

George M. R., et al., Galaxies in X-Ray Groups. I. Robust Membership Assignment and the Impact of Group Environments on Quenching, The Astrophysical Journal, 2011, vol. 749, p. 22

Goodman J., Weare J., Ensemble samplers with affine invariance, Communications in Applied Mathematics and Computational, 2010, vol. 5, p. 65

Haiman Z., et al., Constraints on Cosmological Parameters from Future Galaxy Cluster Surveys, The Astrophysical Journal, 2001, vol. 553, p. 545

Kiiveri K., et al., CODEX weak lensing mass catalogue and implications on the mass-richness relation, Monthly Notices of the Royal Astronomical Society, 2021, vol. 502, p. 1494

Kopylova F. G., Kopylov A. I., Outskirts of Galaxy Clusters A1139, A1314, A1656, A2040, A 2052, A2107: Star-Formation Rate, Astrophysical Bulletin, 2018, pp 267–278

Kopylova F. G., Kopylov A. I., Galaxy Clusters and Their Outskirts: the “Red Sequence”, Star Formation Rate, Stellar Mass, Astrophysical Bulletin, 2019, vol. 74, p. 365

Kopylova F. G., Kopylov A. I., The splashback radius of groups and clusters of galaxies at low redshifts, The Multifaceted Universe: Theory and Observations - 2022 (MUTO2022), 2023

Mendes de Oliveira C., et al., The Southern Photometric Local Universe Survey (S-PLUS): improved SEDs, morphologies, and redshifts with 12 optical filters, Monthly Notices of the Royal Astronomical Society, 2019, vol. 489, p. 241

More S., et al., THE SPLASHBACK RADIUS AS A PHYSICAL HALO BOUNDARY AND THE GROWTH OF HALO MASS, The Astrophysical Journal, 2015, vol. 810, p. 16

More S., et al., Detection of the Splashback Radius and Halo Assembly Bias of Massive Galaxy Clusters, The Astrophysical Journal, 2016, vol. 825, p. 39

Navarro J. F., Frenk C. S., White S. D. M., The Structure of Cold Dark Matter Halos, The Astrophysical Journal, 1996, vol. 462, p. 563

Navarro J. F., Frenk C. S., White S. D. M., A Universal Density Profile from Hierarchical Clustering, The Astrophysical Journal, 1997, vol. 490

Pierre M., Pacaud F., Adami C., et al., The XXL Survey: I. Scientific motivations â XMM-Newton observing plan â Follow-up observations and simulation programme, Astronomy & Astrophysics, 2016, vol. 592, p. A1

Pratt G. W., et al., The Galaxy Cluster Mass Scale and Its Impact on Cosmological Constraints from the Cluster Population, Space Science Reviews, 2019, vol. 215, p. 25

Umetsu K., et al., Cluster-galaxy weak lensing, The Astronomy and Astrophysics Review, 2020a, vol. 28, p. 7

Umetsu K., et al., Weak-lensing Analysis of X-Ray-selected XXL Galaxy Groups and Clusters with Subaru HSC Data, The Astrophysical Journal, 2020b, vol. 890, p. 148

Vikhlinin A., et al., Chandra Cluster Cosmology Project III: Cosmological Parameter Constraints, The Astrophysical Journal, 2009, vol. 692, p. 1060

Voges W., et al., The ROSAT all-sky survey bright source catalogue, Astronomy & Astrophysics, 1999, vol. 349, p. 389

Wang Y., et al., The SDSS galaxy angular two-point correlation function, The Astrophysical Journal, 2013, vol. 432, p. 1961